

3D-QSAR, Docking and Molecular Dynamics Simulation Study of C-Glycosylflavones as GSK-3 β Inhibitors

Suparna Ghosh¹, Seketoulie Keretsu¹, and Seung Joo Cho^{1,2*}

Abstract

Abnormal regulation, hyperphosphorylation, and aggregation of the tau protein are the hallmark of several types of dementia, including Alzheimer's Disease. Increased activity of Glycogen Synthase Kinase-3 β (GSK-3 β) in the Central Nervous System (CNS), increased the tau hyperphosphorylation and caused the neurofibrillary tangles (NFTs) formation in the brain cells. Over the last two decades, numerous adenosine triphosphate (ATP) competitive inhibitors have been discovered that show inhibitory activity against GSK-3 β . But these compounds exhibited off-target effects which motivated researchers to find new GSK-3 β inhibitors. In the present study, we have collected the dataset of 31 C-Glycosylflavones derivatives that showed inhibitory activity against GSK-3 β . Among the dataset, the most active compound was docked with the GSK-3 β and molecular dynamics (MD) simulation was performed for 50 ns. Based on the 50 ns MD pose of the most active compound, the other dataset compounds were sketched, minimized, and aligned. The 3D-QSAR based Comparative Molecular Field Analysis (CoMFA) model was developed, which showed a reasonable value of $q^2=0.664$ and $r^2=0.920$. The contour maps generated based on the CoMFA model elaborated on the favorable substitutions at the R₂ position. This study could assist in the future development of new GSK-3 β inhibitors.

Keywords: Alzheimer's Disease, Kinase, Molecular Docking, Molecular Dynamics, MM/PBSA, CoMFA

Introduction

Alzheimer's Disease (AD) is a known neurodegenerative disorder and common to the aging population. AD patients developed tau lesions in the somas and dendrites due to the aberrant phosphorylation and mislocalization of the tau protein, which is crucial for maintaining the structural integrity of microtubules in the neural cells^[1-3]. The formation of β -amyloid (A β) peptide with tauopathies was considered as the initiator of AD pathogenesis^[2]. Recent studies elucidated that A β deposition triggered the positive regulation of the Glycogen synthase kinase-3 (GSK-3 kinase) by preventing its inhibitory phosphorylation^[4-6]. The GSK-3 is an atypical serine/threonine kinase enzyme that has recently been characterized as a regulator of tau hyper-

phosphorylation in AD. There are two different isoforms of GSK-3 in mammals, namely GSK-3 α and GSK-3 β , where are highly conserved in their catalytic domain and largely redundant in multiple cell signaling pathways. GSK-3 β differs from the GSK-3 α at the C-terminus domain and is inhibited upon phosphorylation at residue Ser9 instead of Ser21 in GSK-3 α ^[7,8]. Between them, GSK-3 β was identified as the major dominating kinase for tau hyperphosphorylation in AD patients and transgenic animal models^[9,10]. Tau protein hyperphosphorylation by hyperactive GSK-3 β was found in more than 70% of the AD brain^[11,12]. Hence, it is necessary to design and develop inhibitors against GSK-3 β . Several adenosine triphosphate (ATP) competitive inhibitors that target GSK-3 β have been developed. However, the off-target selection of these inhibitors remained a significant concern.

In recent studies, natural compounds and their semi-synthetic derivatives have been taken into account for developing selective and irreversible GSK-3 β inhibitor^[13,14]. Liang et al. showed the competitive inhibition of the 31 natural and semi-synthetic C-Glycosylflavone derivatives against GSK-3 β . These compounds exhib-

¹Department of Biomedical Sciences, College of Medicine, Chosun University, Gwangju 501-759, Korea

²Department of Cellular Molecular Medicine, College of Medicine, Chosun University, Gwangju 501-759, Korea

*Corresponding author : chosj@chosun.ac.kr

(Received : October 2, 2020, Revised : November 11, 2020, Accepted : November 28, 2020)

ited a wide range of activities (i.e., IC₅₀ 0.59 \pm 0.04 μ M to 5153 \pm 31 μ M) and were taken for our current study^[15]. The compound C30 which showed the highest activity was docked with the target GSK-3 β to elucidate the key molecular interactions within the substrate-binding site. After that, the MD simulation was performed to study the dynamic interactions between C30 and GSK-3 β . The CoMFA models were developed to explore the structure-activity relations of the GSK-3 β inhibitors.

Methodology

Molecular Docking

A series of 31 GSK-3 β inhibitors based on C-Glycosylflavones have been chosen for this study.¹⁵ The reported inhibitory concentration (IC₅₀) values were converted into -logIC₅₀ (pIC₅₀) values. The most active compound (C30, pIC₅₀= 6.22) was sketched and minimized using tripos forcefield in SYBYL-X 2.1. The crystal structure of GSK-3 β (PDB ID: 1PYX)^[16] was collected from the protein databank (www.rcsb.org) and eliminated all the water molecules, ions, and small molecules. The missing residues and loops were modeled using MODELLER^[17] and treat as a receptor for the docking study. Docking between GSK-3 β and C30 was performed using AutodockTools^[18] described in an earlier study^[19]. The grid-box dimension was set to 60 \times 65 \times 65 around the active site of the receptor, whereby the Lamarckian genetic algorithm^[20] was applied as a search method for the ligand-binding inside the pocket. The 100 runs of docking evaluation were carried out, and the binding conformations of the ligand were clustered based on the similarity of docked position. The cluster-1 conformation of the protein-ligand complex was selected for the molecular dynamics study and MM/PBSA calculation.

Molecular Dynamics (MD) Simulation and Data Analysis

The GROMACS-2020^[21] package was used for molecular dynamics simulation of protein-ligand complex applying the CHARMM36^[22] forcefield. The CHARMM general forcefield (CGenFF)^[23] was used to generate the ligand topology file. The C30-GSK-3 β complex was then immersed into a cubic box with TIP3P water model. The box padding dimension was

kept to 10 Å from the complex and further neutralized by the addition of 13 Cl⁻ ions. The overall system was energy minimized by 100 ps steepest descent method, followed by the 100 ps at a constant substance, volume, and temperature (NVT) equilibration and 100 ps at a constant substance, pressure, and temperature (NPT) equilibration by position restraining of the protein. Finally, an unrestrained 50 ns MD run was continued at 300K of temperature and 1 bar of pressure. The MD trajectory was analyzed using the in-built Gromacs packages. Finally, protein-ligand binding energy was calculated by molecular mechanics energies combined with the Poisson-Boltzmann and surface area continuum solvation (MM/PBSA) method using the *g_mmpbsa* package^[24] described here in an earlier study^[25].

CoMFA

The conformation of C30 from the 50 ns MD trajectory was collected to sketch the other compounds of the dataset. All the compounds were charged (Gasteiger charge) and optimized by Tripos forcefield^[26] in SYBYL-X 2.1, described previously^[27-29]. The compounds were aligned based on the common substructure and proceed further for the CoMFA study. The electrostatic and steric potential energy terms were calculated for each model in CoMFA by probing the 3D-grid space around the sp³ hybridized carbon atom (charge +1). Then the Leave-One-Out (LOO) method was used to cross-validate the predictive ability of the 3D-QSAR model. The partial least square analysis (PLS) was calculated between the dependent and independent variables to establish the structure-activity relationship^[30,31]. Based on the optimum number of components (ONC) the non-cross validated analysis was done to generate the final CoMFA model with reasonable *q*² and *r*² values.

Results and Discussions

Molecular Docking Analysis

Molecular docking result of the C30-GSK-3 β complex was analyzed by AutoDockTools. Protein-ligand complex from the cluster-1 scored -9.84 Kcal/mol with five hydrogen bond formation and was selected to examine the molecular interaction. In the active site, Ile62, Asn64, Ser66, Val70, Lys85, Asp181, Lys183, Leu188, Cys199, and Asp200 were critical for ligand interactions. The residues Asn64, Ser66, Asp181,

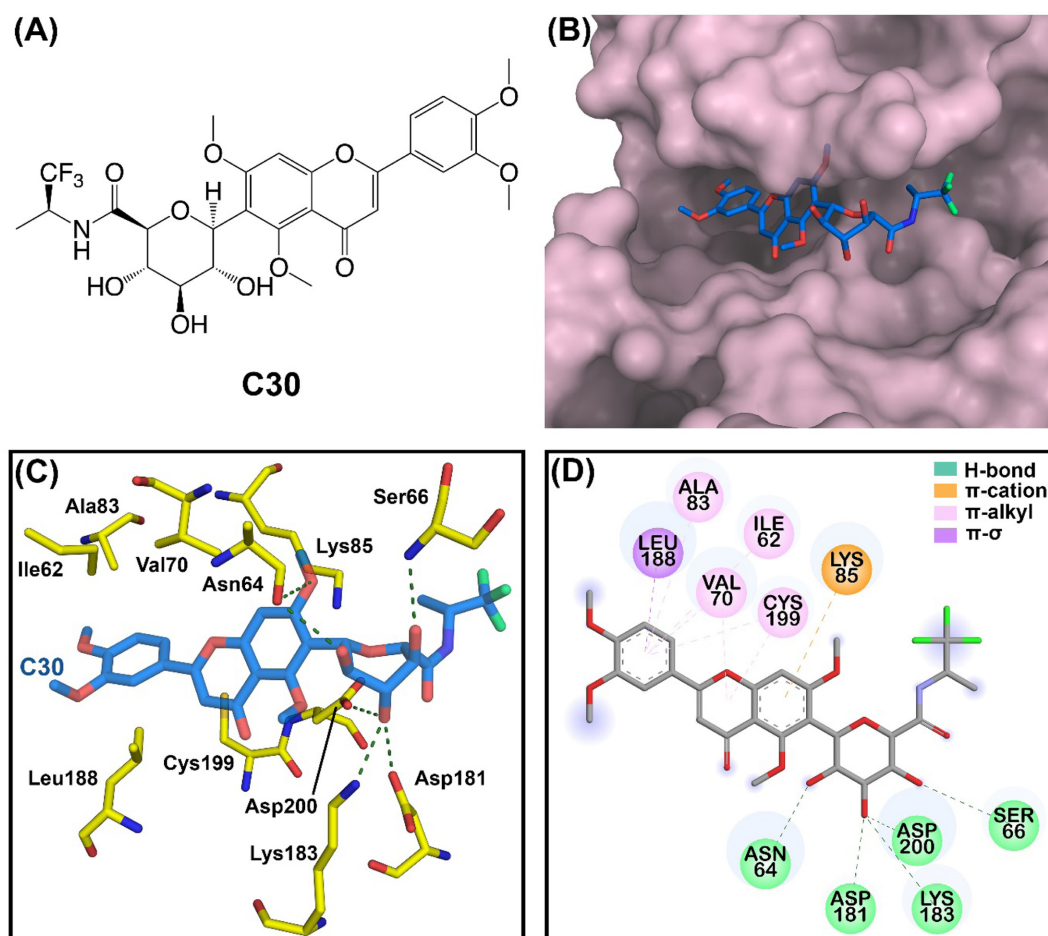


Fig. 1. (A) The molecular structure of the most active compound C30. (B) C30 docked pose in the GSK-3 β active site cavity. (C) Molecular interaction analysis after docking with C30 and GSK-3 β , and (D) 2D ligand interaction map.

Lys183, and Asp200, formed H-bond interaction with three hydroxyl groups of the tetrahydropyran ring of C30. Besides, residues Ile62, Val70, and Ala83, Cys199 formed π -alkyl and π - σ interaction with the catechol B-ring center of the C-Glycosylflavone. Lys85 formed π -cation interaction with the C-Glycosylflavone core. The details interactions have been summarized in Figure 1. The ligand alignment and interaction with residues were similar to the interactions observed in the crystal structures IPYX and 6HK3^[32]. However, no interactions were found between the trifluoropropane group of C30 and the surrounding residues.

MD Simulation and MM/PBSA Analysis

MD simulation of the C30-GSK-3 β complex was

performed for 50 ns. Multiple ligand RMSDs of C30 based on the structures of the ligand at 0 ns, 10 ns, and 30 ns of the MD trajectory as references are shown in Figure 2(C). The RMSD plots suggested the ligand underwent a major conformational change during the first 2 ns. The RMSD plots plateaued after the initial 2 ns of the production run suggesting stabilization of the ligand position. Comparison of the ligand position at 0 ns and 50 ns trajectories Figure 2(A) and 2(B) showed that the -CF₃ moiety shifted from its initial position and formed new interactions with Tyr221 and Tyr222. The -CF₃ moiety was stabilized at the binding site by forming π -anion interaction with Tyr221. At 50 ns, compound C30 formed the hydrogen bond interaction with the residue Gln185, Asn186, and Lys188 and the hydro-

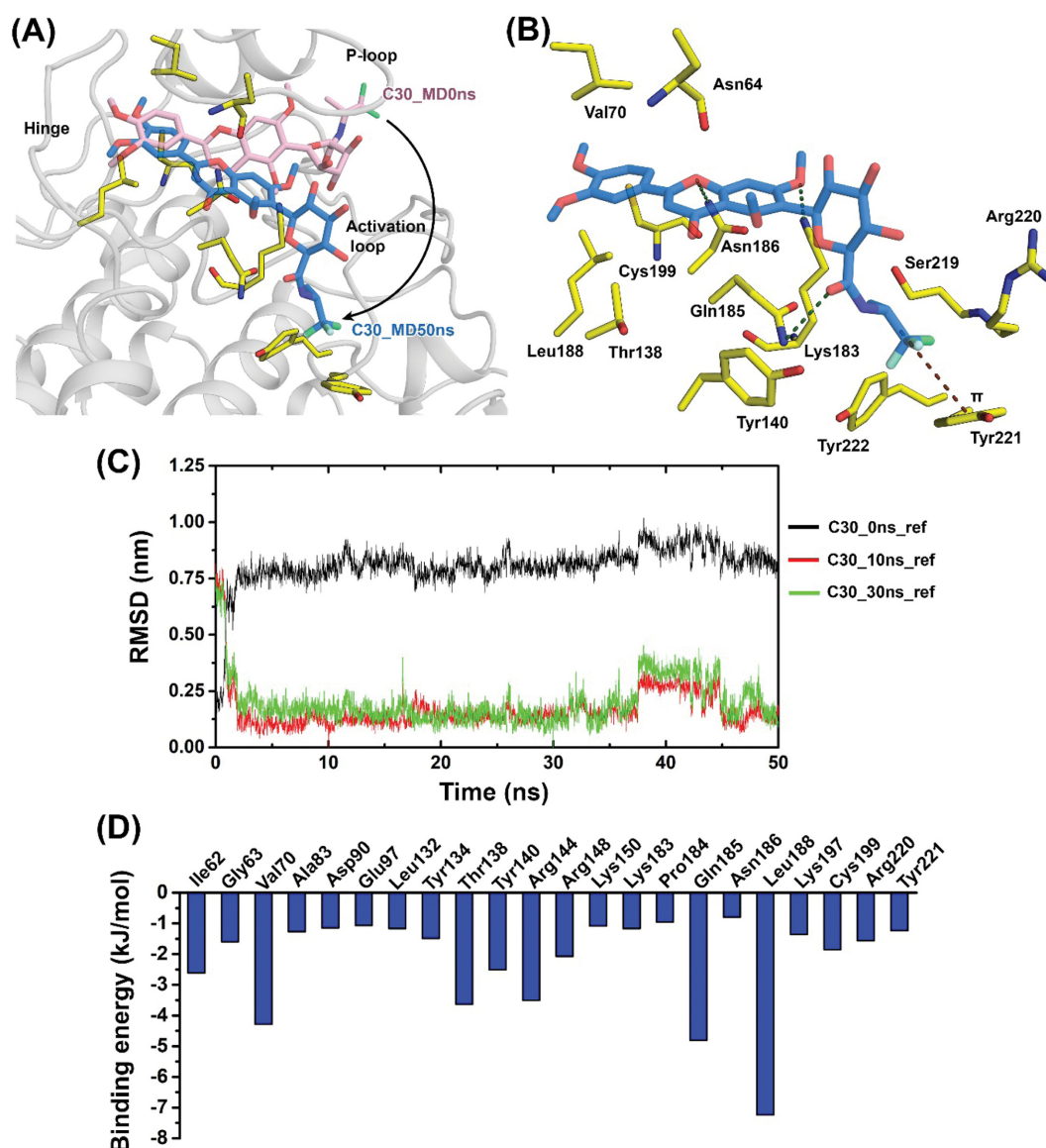


Fig. 2. (A) Ligand position at 0 ns and 50 ns of MD simulation. (B) Molecular interaction of C30 with the active site residues at 50 ns. (C) RMSD analysis of C30, measured based on the position taken at 0 ns (C30_0ns_ref), 10 ns (C30_10ns_ref) and 30 ns (C30_30ns_ref).

phobic interaction with the residue Val70, Leu188, Thr138, and Tyr140.

The final 3 ns of the MD trajectory were collected for binding energy (BE) calculation. BE calculation was done using the *g_mmpbsa* package and summarized in Table 2. The van der Waals interactions and electrostatic interactions played a significant role in total BE

energy, which was found to be -54.60 kJ/mol. The residues, Val70, Thr138, Arg144, Gln185, Leu188, were the major BE contributing residues with BE values of -4.28 kJ/mol, -3.63 kJ/mol, -3.50 kJ/mol, -4.80 kJ/mol, and -7.24 kJ/mol respectively. The detailed analysis was depicted in Figure 2(D).

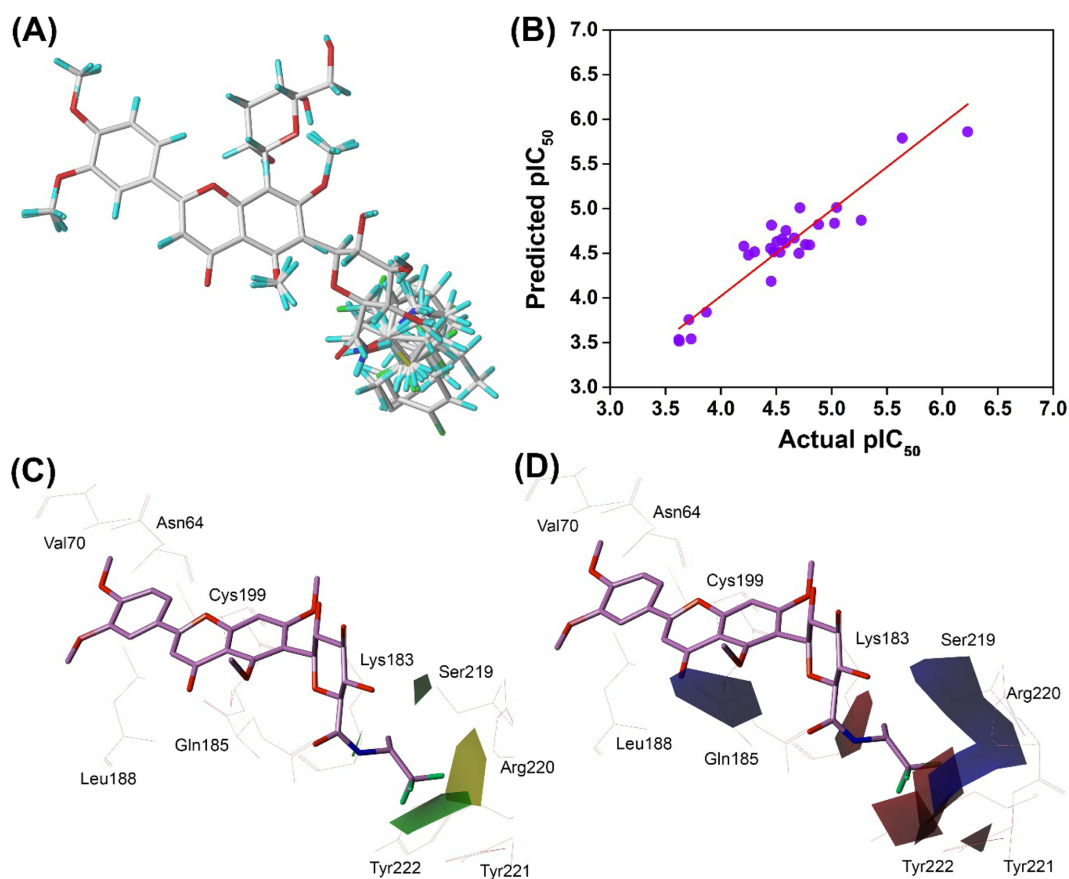


Fig. 3. (A) Data set alignment by making C30 as a template. (B) Scatterplot diagram of the CoMFA model to show the actual vs. predicted pIC_{50} . (C) Steric and (D) Electrostatic contour map from the CoMFA analysis.

CoMFA Model Study

Based on the conformation of C30 at 50 ns, the rest of the compounds were drawn, applied Gasteiger charges, and minimized in SYBYL-X 2.1. All the compounds were aligned by taking C30 as a template. The aligned compounds were shown in Figure 3(A). Chemical structures and their respective pIC_{50} values were given in Table 1. The generated CoMFA model showed the q^2 and r^2 values of 0.664 and 0.920 respectively, at the ONC of 4. The detailed statical analysis was provided in Table 3. The steric and electrostatic field contribution was found to be 81% and 19%, respectively. The statistical results indicated a reasonable predictive ability of the CoMFA model. The actual vs. predicted pIC_{50} values of the compounds and their residuals were tabulated in Table 4. The scatterplot between the predicted and actual pIC_{50} was shown in Figure 3(B).

Compound C4 and C19 were set as outliers (assigned by *) due to their high residual values.

Steric and Electrostatic contour maps from the CoMFA analysis were shown in Figure 3(C) and (D) by taking the most active compound C30 as a reference. The green contour signifies favorable bulky substitution, whereas the yellow contour indicates an unfavorable one. Similarly, the blue contour favored the positive charge substitution, whereas the red contour favored negative charge substitution. A green and red contour map was found near R_2 position, indicating the bulky and electronegative group is favorable at this site. Most active compound C30 and second most active compound C31 poses (*S*)- CF_3 and (*R*)- CF_3 substitution in their R_2 position. But, C30 has more negatively charged $-CF_3$ towards the Tyr221 (*S*-configuration) and showed higher activity compared to C31. Compounds

Table 1. Structure of the C-Glycosylflavones and their pIC₅₀ values for GSK-3 β

Structure A						
Compounds	Structure	R ₁	X ₁	X ₂	R ₂	GSK-3 β (pIC ₅₀)
1		H	H ₂	O	H	3.37
2						3.71
3						2.28
*4						5.50
5	A	CH ₃	H ₂	NH	H	3.62
6	A	CH ₃	O	NH	H	3.62
7	A	CH ₃	O	NH	CH ₃	3.86
8	A	CH ₃	O	NH		4.53
9	A	CH ₃	O	NH		5.26
10	A	CH ₃	O	NH		4.47

Table 1. Continued

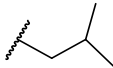
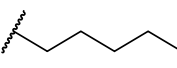
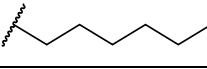
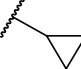

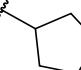
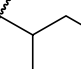
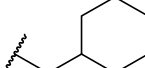
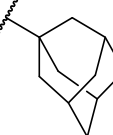
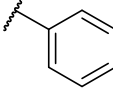
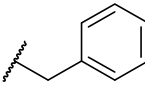
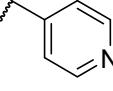
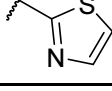
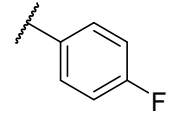
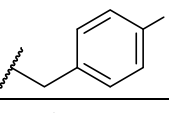
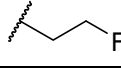
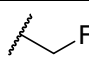
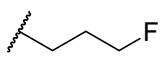
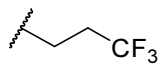
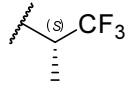
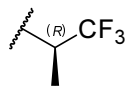
11	A	CH ₃	O	NH		4.50
12	A	CH ₃	O	NH		4.55
13	A	CH ₃	O	NH		5.02
14	A	CH ₃	O	NH		4.58
15	A	CH ₃	O	NH		4.20
16	A	CH ₃	O	NH		4.88
17	A	CH ₃	O	NH		5.04
18	A	CH ₃	O	NH		4.58
*19	A	CH ₃	O	NH		4.47
20	A	CH ₃	O	NH		4.70
21	A	CH ₃	O	NH		4.80
22	A	CH ₃	O	NH		4.44
23	A	CH ₃	O	NH		4.45

Table 1. Continued

24	A	CH ₃	O	NH		4.25
25	A	CH ₃	O	NH		4.66
26	A	CH ₃	O	NH		4.45
27	A	CH ₃	O	NH		4.71
28	A	CH ₃	O	NH		4.30
29	A	CH ₃	O	NH		4.76
30	A	CH ₃	O	NH		6.22
31	A	CH ₃	O	NH		5.63

*Outliers

Table 2. Summary of MM/PBSA binding energy evaluation

Energy term	Binding Energy contribution
Van der Waal energy	-192.12 \pm 19.82 kJ/mol
Electrostatic energy	-48.67 \pm 15.54 kJ/mol
Polar solvation energy	210.40 \pm 28.47 kJ/mol
SASA energy	-24.21 \pm 1.75 kJ/mol
Total Binding energy	-54.60 \pm 11.99 kJ/mol

Table 3. Statistical summary of the CoMFA model

Parameters	CoMFA MODEL
q^2	0.664
ONC	4
SEP	0.443
r^2	0.920
SEE	0.217
F value	68.858
Steric contribution	81%
Electrostatic contribution	19%

q^2 : cross-validated correlation coefficient; ONC: optimum number of components; SEP: standard error of prediction; r^2 : non-cross-validated correlation coefficient; F-value: F-test value; SEE: standard error of estimation.

C1, C2, C3, C5, and C7 were not bearing any bulky substitution and displayed lower activity values than the compounds C16, C17, C18, C21, C22, and C23, which bore bulky substitutions. Compound C27 and C29 have the electronegative -CF₃ towards the Tyr221 and Tyr220, compared to C26 and C28, having only single -F. This substitution could be the reason behind the higher activity values of C27 and C29 compared to C26 and C28 against GSK-3 β inhibition. The contour map analysis suggested that compounds C30, C31, C16, and C17 expressed higher activity values among the dataset compounds due to the favorable substituents.

Table 4. Actual vs predicted pIC_{50} values and their residuals generated from the CoMFA analysis

Compounds	IC_{50} (μ M)	Actual pIC_{50}	CoMFA	
			Predicted pIC_{50}	Residuals
1	184.9 \pm 1.4	3.37	3.54	0.19
2	194.1 \pm 1.0	3.71	3.75	-0.04
3	5153 \pm 31	2.28	2.39	-0.10
4	3.1 \pm 1.3	5.50	3.08	2.42
5	239.2 \pm 1.2	3.62	3.53	0.08
6	237.3 \pm 1.4	3.62	3.51	0.10
7	135.0 \pm 1.3	3.86	3.84	0.02
8	29.2 \pm 1.1	4.53	4.51	0.02
9	5.4 \pm 0.1	5.26	4.86	0.39
10	33.3 \pm 1.1	4.47	4.51	-0.03
11	31.1 \pm 1.2	4.50	4.63	-0.12
12	28.0 \pm 1.1	4.55	4.65	-0.10
13	9.4 \pm 0.9	5.02	4.83	0.19
14	25.8 \pm 1.1	4.58	4.75	-0.16
15	61.9 \pm 1.2	4.20	4.57	-0.37
16	13.1 \pm 1.1	4.88	4.82	0.06
17	9.0 \pm 1.3	5.04	5.01	0.03
18	26.0 \pm 1.2	4.58	4.61	-0.03
19	33.5 \pm 0.8	4.47	5.45	-0.97
20	19.7 \pm 1.1	4.70	4.49	0.20
21	15.8 \pm 1.2	4.80	4.59	0.20
22	35.6 \pm 1.3	4.44	4.55	-0.10
23	35.1 \pm 1.0	4.45	4.18	0.26
24	56.2 \pm 1.2	4.25	4.47	-0.22
25	21.7 \pm 1.2	4.66	4.67	-0.01
26	34.8 \pm 1.0	4.45	4.81	-0.35
27	19.3 \pm 0.8	4.71	5.00	-0.29
28	49.5 \pm 1.2	4.30	4.51	-0.21
29	17.2 \pm 0.9	4.76	4.59	0.16
30	0.59 \pm 0.04	6.22	5.86	0.36
31	2.3 \pm 0.5	5.63	5.78	-0.15

Conclusion

We have performed the molecular modeling study on the C-Glycosylflavone derivatives. C-Glycosylflavones are an interesting candidate over the existing inhibitors due to their ease of chemical modification and higher selectivity for the GSK-3 β . In this study, we have performed docking and MD simulation, which showed the critical interactions for binding with GSK-3 β . MM/

PBSA evaluation showed the important residues that contributed to binding energy for ligand binding. The 3D-QSAR based CoMFA model was developed to study the structure-activity relationship. The contour map analysis from CoMFA showed favorable substitution in the R₂ position for steric and electrostatic interactions. This study could help in developing new C-Glycosylflavon based derivatives to inhibit the GSK-3 β for the treatment of AD patients.

Acknowledgment

This study was supported by research funds from Chosun University 2020.

References

- [1] Hoover, B. R.; Reed, M. N.; Su, J.; Penrod, R. D.; Kotilinek, L. A.; Grant, M. K.; Pitstick, R.; Carlson, G. A.; Lanier, L. M.; Yuan, L.-L., Tau Mislocalization to Dendritic Spines Mediates Synaptic Dysfunction Independently of Neurodegeneration. *Neuron* **2010**, *68*, 1067-1081.
- [2] Miller, E. C.; Teravskis, P. J.; Dummer, B. W.; Zhao, X.; Haganir, R. L.; Liao, D., Tau Phosphorylation and Tau Mislocalization Mediate Soluble A β Oligomer-Induced Ampa Glutamate Receptor Signaling Deficits. *European Journal of Neuroscience* **2014**, *39*, 1214-1224.
- [3] Probst, A.; Tolnay, M.; Langui, D.; Goedert, M.; Spillantini, M., Pick's Disease: Hyperphosphorylated Tau Protein Segregates to the Somatoaxonal Compartment. *Acta neuropathologica* **1996**, *92*, 588-596.
- [4] Qu, Z.-S.; Li, L.; Sun, X.-J.; Zhao, Y.-W.; Zhang, J.; Geng, Z.; Fu, J.-L.; Ren, Q.-G., Glycogen Synthase Kinase-3 Regulates Production of Amyloid- β Peptides and Tau Phosphorylation in Diabetic Rat Brain. *The Scientific World Journal* **2014**, *2014*, 878123.
- [5] Reddy, P. H., Amyloid Beta-Induced Glycogen Synthase Kinase 3 β Phosphorylated Vdac1 in Alzheimer's Disease: Implications for Synaptic Dysfunction and Neuronal Damage. *Biochimica et Biophysica Acta (BBA)-Molecular Basis of Disease* **2013**, *1832*, 1913-1921.
- [6] Sofola, O.; Kerr, F.; Rogers, I.; Killick, R.; Augustin, H.; Gandy, C.; Allen, M. J.; Hardy, J.; Lovestone, S.; Partridge, L., Inhibition of Gsk-3 Ameliorates A β Pathology in an Adult-Onset Drosophila Model of Alzheimer's Disease. *PLoS Genet* **2010**, *6*, e1001087.
- [7] Beurel, E.; Grieco, S. F.; Jope, R. S., Glycogen Synthase Kinase-3 (Gsk3): Regulation, Actions, and Diseases. *Pharmacology & therapeutics* **2015**, *148*, 114-131.
- [8] Hernandez, F.; Lucas, J. J.; Avila, J., Gsk3 and Tau: Two Convergence Points in Alzheimer's Disease. *Journal of Alzheimer's disease* **2013**, *33*, S141-S144.
- [9] Medina, M.; Garrido, J. J.; Wandosell, F. G., Modulation of Gsk-3 as a Therapeutic Strategy on Tau Pathologies. *Frontiers in molecular neuroscience* **2011**, *4*, 24.
- [10] Toral-Rios, D.; Pichardo-Rojas, P. S.; Alonso-Vane-gas, M.; Campos-Peña, V., Gsk3 β and Tau Protein in Alzheimer's Disease and Epilepsy. *Frontiers in Cellular Neuroscience* **2020**, *14*.
- [11] Boutajangout, A.; M Sigurdsson, E.; K Krishnamurthy, P., Tau as a Therapeutic Target for Alzheimer's Disease. *Current Alzheimer Research* **2011**, *8*, 666-677.
- [12] Ko, H.-J.; Chiou, S.-J.; Wong, Y.-H.; Wang, Y.-H.; Lai, Y.-L.; Chou, C.-H.; Wang, C.; Loh, J.-K.; Lieu, A.-S.; Cheng, J.-T., Gskip-Mediated Anchoring Increases Phosphorylation of Tau by Pka but Not by Gsk3beta Via Camp/Pka/Gskip/Gsk3/Tau Axis Signaling in Cerebrospinal Fluid and Ips Cells in Alzheimer Disease. *Journal of clinical medicine* **2019**, *8*, 1751.
- [13] Eldar-Finkelman, H.; Martinez, A., Gsk-3 Inhibitors: Preclinical and Clinical Focus on Cns. *Frontiers in molecular neuroscience* **2011**, *4*, 32.
- [14] Khan, I.; Tantray, M. A.; Alam, M. S.; Hamid, H., Natural and Synthetic Bioactive Inhibitors of Glycogen Synthase Kinase. *European journal of medicinal chemistry* **2017**, *125*, 464-477.
- [15] Liang, Z.; Li, Q. X., Discovery of Selective, Substrate-Competitive, and Passive Membrane Permeable Glycogen Synthase Kinase-3 β Inhibitors: Synthesis, Biological Evaluation, and Molecular Modeling of New C-Glycosylflavones. *ACS chemical neuroscience* **2018**, *9*, 1166-1183.
- [16] Bertrand, J.; Thieffine, S.; Vulpetti, A.; Cristiani, C.; Valsasina, B.; Knapp, S.; Kalisz, H.; Flocco, M., Structural Characterization of the Gsk-3 β Active Site Using Selective and Non-Selective Atp-Mimetic Inhibitors. *Journal of molecular biology* **2003**, *333*, 393-407.
- [17] Webb, B.; Sali, A., Comparative Protein Structure Modeling Using Modeller. *Current protocols in bioinformatics* **2016**, *54*, 5.6. 1-5.6. 37.
- [18] Huey, R.; Morris, G. M., Using Autodock 4 with Autodocktools: A Tutorial. *The Scripps Research Institute, USA* **2008**, 54-56.
- [19] Keretsu, S.; Bhujbal, S. P.; Cho, S. J., Docking and 3d-Qsar Studies of Hydrazone and Triazole Derivatives for Selective Inhibition of Grk2 over Rock2. *Letters in Drug Design & Discovery* **2020**, *17*, 618-632.
- [20] Morris, G. M.; Goodsell, D. S.; Halliday, R. S.;

- Huey, R.; Hart, W. E.; Belew, R. K.; Olson, A. J., Automated Docking Using a Lamarckian Genetic Algorithm and an Empirical Binding Free Energy Function. *Journal of computational chemistry* **1998**, *19*, 1639-1662.
- [21] Lindahl, E.; Abraham, M.; Hess, B.; van der Spoel, D., Gromacs 2020 Manual. Version: 2020.
- [22] Huang, J.; MacKerell Jr, A. D., Charmm36 All-Atom Additive Protein Force Field: Validation Based on Comparison to Nmr Data. *Journal of computational chemistry* **2013**, *34*, 2135-2145.
- [23] Vanommeslaeghe, K.; Hatcher, E.; Acharya, C.; Kundu, S.; Zhong, S.; Shim, J.; Darian, E.; Guvench, O.; Lopes, P.; Vorobyov, I., Charmm General Force Field: A Force Field for Drug-Like Molecules Compatible with the Charmm All-Atom Additive Biological Force Fields. *Journal of computational chemistry* **2010**, *31*, 671-690.
- [24] Kumari, R.; Kumar, R.; Consortium, O. S. D. D.; Lynn, A., G_Mmpbsa a Gromacs Tool for High-Throughput Mm-Pbsa Calculations. *Journal of chemical information and modeling* **2014**, *54*, 1951-1962.
- [25] Keretsu, S.; Bhujbal, S. P.; Cho, S. J., Computational Study of Paroxetine-Like Inhibitors Reveals New Molecular Insight to Inhibit Grk2 with Selectivity over Rock1. *Scientific reports* **2019**, *9*, 1-14.
- [26] Clark, M.; Cramer III, R. D.; Van Opdenbosch, N., Validation of the General Purpose Tripos 5.2 Force Field. *Journal of Computational Chemistry* **1989**, *10*, 982-1012.
- [27] Gadhe, C. G.; Kothandan, G.; Cho, S. J., Large Variation in Electrostatic Contours Upon Addition of Steric Parameters and the Effect of Charge Calculation Schemes in Comfa on Mutagenicity of Mx Analogues. *Molecular Simulation* **2012**, *38*, 861-871.
- [28] Gadhe, C. G.; Madhavan, T.; Kothandan, G.; Cho, S. J., In Silico Quantitative Structure-Activity Relationship Studies on P-Gp Modulators of Tetrahydroisoquinoline-Ethyl-Phenylamine Series. *BMC structural biology* **2011**, *11*, 5.
- [29] San Juan, A. A.; Cho, S. J., 3d-Qsar Study of Microsomal Prostaglandin E 2 Synthase (Mpges-1) Inhibitors. *Journal of Molecular Modeling* **2007**, *13*, 601-610.
- [30] Bang, S. J.; Cho, S. J., Comparative Molecular Field Analysis (Comfa) and Comparative Molecular Similarity Index Analysis (Comsia) Study of Mutagen X. *BULLETIN-KOREAN CHEMICAL SOCIETY* **2004**, *25*, 1525-1530.
- [31] Pasha, F.; Cho, S. J.; Beg, Y.; Tripathi, Y., Quantum Chemical Qsar Study of Flavones and Their Radical-Scavenging Activity. *Medicinal Chemistry Research* **2007**, *16*, 408-417.
- [32] Gobbo, D.; Piretti, V.; Di Martino, R. M. C.; Tripathi, S. K.; Giabbai, B.; Storici, P.; Demitri, N.; Giroto, S.; Decherchi, S.; Cavalli, A., Investigating Drug-Target Residence Time in Kinases through Enhanced Sampling Simulations. *Journal of Chemical Theory and Computation* **2019**, *15*, 4646-4659.